TNFR1-mediated senescence and lack of TNFR2-signaling limit human intervertebral disc cell repair in back pain conditions

Authors: Jennifer Gansau[1], Elena Grossi[2,3], Levon Rodriguez [1,4], Minghui Wang[4], Damien M. Laudier[1], Saad Chaudhary[1], Andrew C. Hecht[1], Wenyu Fu[5], Robert Sebra[4], Chuanju Liu[5], James C. Iatridis[1,*]

Affiliations:

[1]Department of Orthopaedics, Icahn School of Medicine at Mount Sinai; New York, NY 10029, USA.

[2]Department of Oncological Sciences, Icahn School of Medicine at Mount Sinai; New York, NY 10029, USA.

[3]Department of Dermatology, Icahn School of Medicine at Mount Sinai; New York, NY 10029, USA.

[4]Department of Genetics & Genomic Sciences, Icahn School of Medicine at Mount Sinai; New York, NY 10029, USA.

[5]Department of Orthopaedics & Rehabilitation, Yale University School of Medicine; New Haven, CT 06510, USA.

*Corresponding author. James C Iatridis

Email: james.iatridis@mssm.edu

Address: Leni and Peter W. May Department of Orthopaedics

One Gustave Levy Place, Box 1188

Icahn School of Medicine at Mount Sinai

New York, NY 10029, USA

Telephone: +1-212-241-1517

ABSTRACT

Poor intervertebral disc (IVD) healing causes IVD degeneration (IVDD) and progression to herniation and back pain. This study identified distinct roles of TNFα-receptors (TNFRs) in contributing to poor healing in painful IVDD. We first isolated IVDD tissue of back pain subjects and determined the complex pro-inflammatory mixture contained many chemokines for recruiting inflammatory cells. Single-cell RNA-sequencing of human IVDD tissues revealed these pro-inflammatory cytokines were dominantly expressed by a small macrophage-population. Human annulus fibrosus (hAF) cells treated with IVDD-conditioned media (CM) underwent senescence with greatly reduced metabolic rates and limited inflammatory responses. TNFR1 inhibition partially restored hAF cell metabolism sufficiently to enable a robust chemokine and cytokine response to CM. We showed that the pro-reparative TNFR2 was very limited on hIVD cell membranes so that TNFR2 inhibition with blocking antibodies or activation using Atsttrin had no effect on hAF cells with CM challenge. However, TNFR2 was expressed in high levels on macrophages identified in scRNA-seq analyses, suggesting their role in repair responses. Results therefore point to therapeutic strategies for painful IVDD involving immunomodulation of TNFR1 signaling in IVD cells to enhance metabolism and enable a more robust inflammatory response including recruitment or delivery of TNFR2 expressing immune cells to enhance IVD repair.

SUMMARY STATEMENT

TNFR1 signaling drives cells towards senesce and muted inflammatory response in painful intervertebral disc degeneration, while limited TNFR2 signaling may limit disc cell repair responses.

53 **INTRODUCTION**

54 Back and neck pain are leading causes of global disability impacting >100 million US
55 adults, leading to missed workdays, massive health care expenditures and contribute to opioid
56 usage, and represents a tremendous global socioeconomical burden (1-4). Intervertebral disc (IVD)
57 herniation involving annulus fibrosus (AF) defects is a direct cause of pain and disability that can
58 predispose to IVD degeneration (IVDD) and result in painful disability (1, 5, 6). Chronic
59 inflammation is a characterizing feature of IVDD and herniation with pro-inflammatory cytokines
60 contributing to progressive IVDD and pain (7-10). Pro-inflammatory cytokines play known roles
61 in IVD matrix catabolism, neurovascular ingrowth, nociception and cellular senescence (8-20).
62 Tumor necrosis factor-alpha (TNFα), interleukin-1 Beta (IL-1β) and interleukin-6 (IL-6) are major
63 cytokines identified in the IVD known to propagate matrix catabolism and nociception, and
64 considered targets for therapeutic strategies (8, 9, 11-14, 20, 21).

65 Human clinical trials and animal studies show promise for TNFα blocking in IVDD, but
66 mixed results prompt a need for further research. In human clinical trials for IVD herniation with
67 radiculopathy, local and systemic administration of TNFα blocking agents, including infliximab,
68 etanercept and adalimumab, showed some promise for pain reduction but remained inconclusive
69 since trials exhibited broad heterogeneity in effects and several showed negative findings (22-28).
70 While a randomized, double-blinded, placebo-controlled trial of 43 patients with disc herniation
71 found some decrease of average back pain using etanercept compared to placebo after 28 weeks,
72 a randomized, controlled trial that enrolled 40 discectomy patients with disc herniation concordant
73 with radicular pain, found infliximab had similar effects as placebo at 3-month follow-up (23, 29).
74 Meanwhile, preclinical animal studies show efficacy with early TNFα blocking with reduced pain
75 and improved IVD degeneration score (13, 30). These mixed clinical and animal results highlight

76 importance of TNFα, but also a need to better understand TNFα signaling and crosstalk between
77 IVD and immune cells (7). Therefore, here, we focus on specific roles of TNFα-receptors.

78 TNFα signaling occurs via 2 receptors: TNFα-receptor 1 (TNFR1) is implicated in the pro-
79 inflammatory response that promote tissue catabolism, and TNFα-receptor 2 (TNFR2) is
80 associated with cell survival and tissue repair/regeneration (31-34). Current treatment strategies
81 involve antibody-based inhibition with a high binding affinity for TNFα and therefore actively
82 prevents TNFα from binding to both TNFR1 and TNFR2 (23, 30, 32, 35, 36). Selective TNFR
83 inhibition shows promise for IVDD since TNFR1$^{-/-}$ mice protected from IVDD while TNFR2$^{-/-}$
84 mice accelerated IVDD (20). The engineered protein Atsttrin is a TNFR2 activator derived from
85 progranulin, and this novel therapeutic was shown in osteoarthritis and IVD organ culture to shift
86 TNFα signaling from TNFR1 to a greater TNFR2 response (37-41). However, these studies need
87 validation in a human model system with a translational strategy.

88 A common strategy for simulating IVDD conditions is supplementation of cell culture
89 media with pro-inflammatory cytokines such as TNFα, IL-1β and IL-6 (10, 37, 42-44). However,
90 painful human IVDD with herniation is known to involve multiple cytokines and chemokines that
91 are collectively responsible for different cellular functions thought to inhibit IVD repair and
92 promote painful responses (8). We therefore applied a human relevant cell culture model system
93 that recapitulated the complex cytokine environment of human IVDD.

94 This study tested the hypotheses that human IVDD involves a complex cytokine mixture
95 that drives IVD cells towards senescence and can be shifted towards a reparative responsive by
96 inhibiting TNFR1 and promoting TNFR2 activity. This study used human tissue and cells from
97 painful IVDD subjects and autopsies, and applied cell culture, bulk RNA-sequencing, single-cell
98 RNA-sequencing (scRNA-seq), gene and protein assays. We determined that the many cytokines

99 and chemokines present in IVDD tissue from surgical subjects were dominantly expressed by a
100 small population of macrophages, and expressed at far lower levels by IVD cells. Next, we showed
101 that IVDD conditioned media (CM) treatment on human AF (hAF) cells *in vitro* had the largest
102 effects inhibiting metabolic rates and promoting senescence. Blocking TNFR1 signaling during
103 CM exposure sufficiently restored hAF cell metabolism to enable a robust pro-inflammatory
104 response. However, blocking TNFR2 and enhancing TNFR2 signaling with Atsttrin during CM
105 exposure had no effects on hAF cells. Finally, we showed TNFR1 is highly expressed by IVD cells
106 and increased with IVDD grade underscoring its importance in IVDD, and we showed that TNFR2
107 was expressed at minimal amounts by IVD cells suggesting limited TNFR2 signaling at below
108 therapeutic levels in IVDD conditions.

109 **RESULTS**

110 **CM contains many cytokines & chemokines dominantly expressed by macrophages**

111 To characterize the IVDD pro-inflammatory microenvironment, human surgical IVD
112 specimens containing both AF and NP portions were collected (Table S1) and cultured in Basal
113 media for 72 hours under constant agitation, leading to cytokine release and generating IVDD
114 derived CM (Fig. 1A). CM cytokines and chemokines were analyzed with a human
115 cytokine/chemokine panel 48-plex discovery Assay® Array, with pro-inflammatory cytokines
116 (e.g., IL-1β, IL-6, TNFα), anti-inflammatory cytokines (e.g., IL-1RA, IL-4, IL-10, IL-13), and
117 chemokines (e.g., MIP-1α/CCL3, MIP1β/CCL4, MCP-1/CCL2 and MCP-3/CCL7) detected (Fig.
118 1B, Table S2). To determine the cells producing these factors, we performed scRNA-seq on cells
119 isolated from 5 herniated IVD specimens containing AF and NP regions from 3 subjects
120 undergoing Anterior cervical discectomy and fusion (ADF) procedure (1 male, 2 female) (Fig. 1A,
121 Fig. S1A, Table S1). The 13,259 cells were analyzed to identify 14 clusters that were annotated
122 using UniCell Deconvolve (Fig. S1), a pre-trained, unbiased, deep learning model system (45).

123 Cell cluster 13 was identified as a small population of macrophages using UniCell and we
124 manually confirmed this annotation as macrophages by evaluating expression of markers including
125 *CD68, CXCL16, C1QB* and *CD14* (Fig. S2A). While these macrophages represent only 0.16% of
126 the cells of the specimens (Fig. S2B), they are highlighted because they expressed the genes
127 translating to the cytokines present in the IVDD CM at high levels (Fig. 1C, Fig. 1D). Specifically,
128 the macrophage cluster contained 217 significantly upregulated genes including *IL1B, CCL3*
129 (*MIP1α*), *CCL3L1* and *CCL4* (*MIP1β*), and emphasized the robustness of its pro-inflammatory
130 roles compared to all other cell clusters (Fig. 1E), and this population did not express IVD cell
131 phenotypic markers. Pathway analysis showed macrophage expression pattern was significantly
132 enriched for "TNFα Signaling via NFκB" (Score= 385.8, adj. p-value= 2.27×10^{-13}), "Inflammatory
133 Response" (Score= 123.6, adj. p-value= 5.89×10^{-7}) and "Complement" (Score= 100.3, adj. p-
134 value= 3.22×10^{-6}) (Fig. 1F). M1-macrophage markers were 2.5-fold greater (average of 82%, red
135 dotted line) than M2-macrophage markers (average of 29%, green dotted line) suggesting
136 macrophages were in an M1 pro-inflammatory phenotype with little conversion to M2 reparative
137 phenotype (Fig. 1G, Fig. S2C). Macrophages expressed the cytokines found in CM at high levels
138 suggesting a role contributing to the CM profiles. Meanwhile, cytokines in CM were expressed by
139 IVD cells at levels that were considerably lower than by the macrophages. We conclude IVDD
140 tissue from back pain subjects contains a complex 'cocktail' of pro-inflammatory cytokines and
141 chemokines dominantly expressed by a very small population of macrophages enriched for TNFα
142 signaling.

143 **CM inhibited hAF cell metabolism and produced a muted inflammatory response**

144 We next used CM to challenge hAF cells in the development of an *in vitro* model system
145 representing the complex IVDD cytokine microenvironment (Fig. 2). Use of the CM cytokine

146 ‘cocktail’ was significant since most IVD cell culture models challenge cells with a single cytokine
147 (most commonly TNFα or IL-1β). The 2D hAF cell culture model system maintains the elongated
148 phenotype of native AF cells and simplifies cellular solute transport conditions. CM was applied
149 in a 2-part study on dosing and timing, and compared with Basal media. CM was generated from
150 specimens collected and pooled from 9 subjects (Table S1). The dosing study applied increasing
151 CM concentrations (Basal, 25%, 50% and 100% CM) to hAF cells cultured for 24 hours in Basal
152 media (Fig. 2A). CM concentration decreased the number of hAF cells visible in culture (Fig. 2B)
153 and significantly decreased hAF cell metabolic activity (Fig. 2C). While increasing CM dose
154 reduces relative nutrients available, we confirmed glucose concentration in all CM conditions was
155 several folds greater than required for hAF cells under these culture conditions (46) to confirm
156 results were related to cytokine concentration changes.

157 We next performed a timing study with 100% CM (Fig. 2A) and showed CM treatment
158 again reduced cell numbers and MTT at 24-hours and further decreased cell numbers with more
159 granulated cell morphology with elongated stress fibers (Fig. 2D), and reduced MTT at 72 hours
160 (Fig. 2E). *COL1A1* and *ADAMTS4* were also significantly decreased with CM at both time points
161 (Fig. 2F), although CM exposure did not result in significantly altered pro-inflammatory cytokines
162 (Fig. S3C). *TNFRSF1A* and *TNFRSF1B* (genes for TNFR1 and TNFR2, respectively) were
163 significantly increased with CM at 24 hours but then significantly decreased at 72 hours (Fig. 2G).
164 Even though *TNFRSF1A* and *TNFRSF1B* levels were both responsive to CM treatment, we show
165 *TNFRSF1B* was expressed at extremely low levels 100-1000x times below *TNFRSF1A* expression
166 levels (Fig. 3H). Overall, we conclude that CM causes hAF cells to have reduced metabolic rate,
167 and a limited pro-inflammatory response. We also identified that CM altered TNFR1 and TNFR2

168 signaling, yet, hAF cells expressed *TNFRSF1B* at levels orders of magnitudes lower than
169 *TNFRSF1A*.

170 **TNFR1 blocking enhanced hAF cell metabolic and pro-inflammatory response while**
171 **TNFR2 blocking and Atsttrin had no effects**

172 Since CM altered expression levels of *TNFRSF1A* and *TNFRSF1B* in hAF cells, we next
173 evaluated their functional roles on hAF cells challenged by CM using blocking antibodies αTNFR1
174 and αTNFR2, and using TNFR2 activator Atsttrin with bulk RNA-Seq analyses. CM was
175 supplemented with inhibiting antibodies at 10 μg/mL and Atsttrin at 200 ng/mL, and hAF cells
176 were cultured for 24 hours (Table 1, Fig. 3A). Blocking TNFR1 partially rescued hAF cells from
177 CM with improved cell morphology (Fig. 3B) and significantly increased MTT ($p < 0.05$, Fig. 3C)
178 compared to CM ($p<0.05$) and αTNFR2 ($p<0.01$), although αTNFR1 was significantly reduced
179 compared to Basal ($p<0.05$, Fig. 3C). While MTT values were only partially rescued for αTNFR1,
180 it was sufficient to promote a substantially different transcriptome with robust pro-inflammatory
181 transcriptomic profile (Fig. 3D & 3E). Specifically, Bulk RNA-seq with principal component
182 analysis (PCA) on transcriptome showed three distinct clusters (Basal, αTNFR1 and the three
183 remaining groups – CM, αTNFR2, Atsttrin) (Fig. 3D). The αTNFR1 robustly increase in pro-
184 inflammatory cytokines expression shown on the top 50 DEGs on the heatmap (Fig. 3E).
185 *TNFRSF1A* expression was significantly upregulated in CM, αTNFR2 and Atsttrin compared to
186 Basal, and significantly inhibited for αTNFR1, validating the importance of TNFR1 signaling
187 under CM conditions and successful blocking by αTNFR1 (Fig. 3F). *TNFRSF1B* expression was
188 not affected by CM, αTNFR2, or Atsttrin suggesting little TNFR2 signaling under the complex
189 cytokine challenge of CM.

190 CM, αTNFR2 and Atsttrin groups had nearly identical responses for all assays, suggesting
191 little TNFR2 signaling. Specifically, CM, αTNFR2 and Atsttrin exhibited more floating cells
192 compared to Basal and αTNFR1 (pink arrows, Fig. 3B) and significantly lower MTT relative
193 optical density compared to Basal (Fig. 3C). The majority of the variability on the green cluster on
194 PCA was from donor differences with very little variability from treatment group (CM, αTNFR2
195 or Atsttrin) (Fig. 3D). The heatmap of the top 50 differentially expressed genes (DEGs) similarly
196 showed distinct patterns for Basal, αTNFR1 and CM groups and near identical patterns for CM,
197 αTNFR2 and Atsttrin groups (Fig. 3E). While the Z-score for *TNFRSF1B* was significantly
198 increased with αTNFR1 inhibition (Fig. 3F), we believe TNFR2 signaling may not have biological
199 impact in IVD since it was not reduced by αTNFR2, since CM, αTNFR2 and Atsttrin had nearly
200 identical results across assays, and because qPCR showed *TNFRSF1B* expression levels were 100-
201 1000x lower than *TNFRSF1A* (Fig. 2H). Overall, we have 3 key findings. First, CM significantly
202 inhibited metabolic rate of hAF cells. Second, TNFR1 inhibition partially restored hAF cell
203 metabolic rates sufficiently to enable a robust pro-inflammatory response. Third, results suggest
204 little functional role for TNFR2 signaling in hAF cells exposed to CM. The lack of responsiveness
205 of TNFR2 inhibition adds to our data on lack of TNFR2 expression in IVD cells in supporting our
206 hypothesis that IVD cells have limited TNFR2 signaling.

207 **CM inhibited hAF DNA replication while αTNFR1 shifted hAF cell pro-inflammatory**
208 **response to predict enhanced immune cell recruitment**

209 Basal, αTNFR1 and CM were analyzed further with gene set enrichment analysis (GSEA)
210 and network analysis with ingenuity pathway analyses (IPA) because of the large transcriptional
211 differences and to discern how TNFR1 modulation shifted the response of hAF cells to the CM
212 challenge. Meanwhile αTNFR2 and Atsttrin were not further analyzed since they had negligible

213 transcriptomic differences from CM. CM significantly downregulated 509 DEGs and significantly
214 upregulated 762 DEGs compared to Basal (Fig. 4A). The most significantly downregulated DEGs
215 were of the minichromosome maintenance gene family (*MCM* genes), which play roles in DNA
216 replication (47). GSEA further showed CM had the highest scores for depleting biological
217 processes related to Cell cycle and DNA replication while inflammatory responses were most
218 significantly enriched (Fig. 4B). The αTNFR1 treatment compared to CM significantly
219 downregulated 490 DEGs, and significantly upregulated 545 DEGs (Fig. 4C). GSEA predicted
220 these DEGs to be enriched for IL-27 mediated signaling (Fig. 4D), which has multiple effects in
221 modulating inflammatory responses (48). Additional enriched biological processes were related to
222 Regulation of Neuroinflammatory Response, and Response to Cytokine, demonstrating a shift in
223 the inflammatory pathways activated by CM (Fig. 4D). Processes related to Presynaptic
224 Endocytosis and Regulation of Calcium Ion Dependent Exocytosis were significantly depleted,
225 suggesting TNFR1 blocking could influence communication with the peripheral nervous system
226 as compared to CM. The αTNFR1 group (which also contained CM) compared to Basal
227 significantly downregulated 448 DEGs and significantly 1072 DEGs with *NFKB2*, *TNFAIP3* and
228 *CCL5* among the highest fold change (FC) DEGs (Fig. 4E). The αTNFR1 treated CM condition,
229 therefore enriched biological processes related to cellular response to type 1 interferon, cytokine-
230 mediated signaling pathways, and inflammatory response compared to Basal and depleted
231 processes related to axonogenesis and axon guidance (Fig. 4F). Network analysis using QIAGEN
232 IPA predicted that CM would activate hAF cell senescence and inhibit proliferation compared to
233 Basal (Fig. 4G). Meanwhile network analyses predicted that hAF cells treated with αTNFR1 would
234 enhance cell activity and processes related to immune cell recruitment compared to CM (Fig. 4H).
235 Further, αTNFR1 treated CM predicted inhibition of SOCS1, a suppressor of cytokine signaling,

236 compared to Basal, to promote the robust pro-inflammatory response observed. Overall, CM
237 depletes DNA replication and enriches inflammation. While, αTNFR1 enabled enhanced the hAF
238 cell pro-inflammatory response to CM and predicted immune cell recruitment.

239 **CM inhibited cell cycle and promoted senescence that was partially restored with αTNFR1**

240 The reduced metabolic rates of hAF cells with increased CM concentration and reductions
241 with αTNFR1 motivated a closer investigation of the cell proliferation, apoptosis, and cell cycle
242 for Basal, αTNFR1, and CM groups (Fig. 5A). We considered cell cycle genes transcription
243 patterns relevant across multiple cellular models across different biological contexts (49, 50), and
244 determined that CM significantly downregulated hAF genes related to each phase of the cell cycle
245 compared to Basal (Fig. 5B). Furthermore, CM caused hAF cells to be express G0 markers
246 indicative of quiescence (i.e., downregulation of *FOXM1, BIRC5* and *H2AFZ* and upregulation of
247 *PFDN5* and *RPS14*) (50) relative to Basal. Blocking TNFR1 led to a pattern of cell cycle markers
248 between CM and Basal, suggesting a partial cell cycle recovery. *MKI67*, the gene coding for the
249 proliferation marker KI67, was significantly decreased for hAF cells in CM ($p<0.0001$), while
250 αTNFR1 was significantly different from CM and Basal (Fig. 5C). The senescence marker SA-β-
251 Gal (Fig. 5D) was significantly increased in hAF cells in CM compared to Basal, and compared to
252 αTNFR1 (Fig. 5E), again suggesting a partial recovery by αTNFR1. The apoptosis marker
253 Caspase-3 (Casp3) (Fig. 5F) showed no difference in co-localization of cleaved Casp3 and DAPI
254 using the Pearson's correlation coefficient (PCC) or in fluorescent intensity within the nuclei
255 between groups (Fig. 5G, Fig. 5H), suggesting no changes in apoptosis. Together, transcriptomic
256 and protein assay results indicated that CM downregulated hAF cell cycle markers and increased
257 senescence and not apoptosis, while αTNFR1 partially protected and restored cell cycle from
258 senescence. While the senescence and cell cycle recovery was only partial with αTNFR1, the

259 expression profile (Fig. 3, Fig. 4) showed it was sufficient to enable hAF cells to mount a robust
260 pro-inflammatory response.

261 **TNFR1 increases with IVDD while TNFR2 is expressed only in macrophages**

262 We further analyzed roles of TNFR1 and TNFR2 in IVDs using immunohistochemistry
263 (IHC) on human autopsy samples and scRNA-seq on human IVDD samples. Human IVDs of
264 various degeneration grades (n=14, Rutgers grade 1.3-12) were stained for TNFR1 and TNFR2
265 respectively and the outer AF (oAF) analyzed using HALO Multiplex module (Fig. 6A). TNFR1
266 was found in the cell membrane of oAF cells as expected, and the % positive cells for TNFR1
267 significantly correlated with IVDD Grade (Fig. 6B, Fig. 6C). This significant correlation between
268 TNFR1 protein expression and Rutgers IVDD grade was also found in the inner AF and NP (Fig.
269 S5). TNFR2 only showed faint staining within and around the nuclei of oAF cells suggesting little
270 presence of TNFR2 (Fig. 6B). Furthermore, the % TNFR2 positivity of these faintly stained cells
271 were not affected by IVDD grade in the oAF (Fig. 6D), or inner AF and NP regions (Fig. S5). We
272 used scRNA-seq of human IVDD subjects to further investigate which human IVD cells expressed
273 the genes for TNFR1 and TNFR2. *TNFRSF1A* was expressed in nearly all cells in the scRNA-seq
274 analyses and had particularly high expression levels in AF and NP cells as well as erythrocytes
275 (Fig. 6E, Fig. 6F) supporting its important role in IVD response to IVDD CM conditions. In
276 contrast, *TNFRSF1B* was at extremely low levels in all IVD cell populations (Fig. 6E, Fig. 6F), in
277 line with the extremely low expression levels in hAF cells on qPCR, and faint TNFR2 staining.
278 Interestingly, the small macrophage population expressed *TNFRSF1B* at very high levels and
279 *TNFRSF1A* at negligible levels. Results therefore support our hypotheses that TNFR2 signaling is
280 very low in all IVD cells and further emphasize the importance of TNFR1 signaling in all IVD

281 cells with TNFR1 signaling increasing with IVDD grade. The scRNA-seq also shows importance
282 of TNFR2 signaling in immune cell populations.

283 **DISCUSSION**

284 There is a major need to develop improved therapeutic targets to manage the chronic pro-
285 inflammatory conditions in painful IVDD, and to develop strategies for IVD cell
286 immunomodulation to slow IVDD progression or enhance IVD healing. Here, we use multiple
287 human model systems to understand roles of TNFR1 and TNFR2 in modulating the complex
288 cytokine and chemokine environment of IVDD. We first show that IVDD derived CM contains
289 elevated levels of at least 32 cytokines and chemokines highlighting the complex pro-
290 inflammatory environment with known roles recruiting inflammatory cells. It was notable that
291 these chemokines were dominantly expressed by a small population of macrophages while native
292 IVD cells (present in substantially larger numbers) expressed these pro-inflammatory factors at
293 much lower levels. CM treatment on hAF cells had the largest effects reducing metabolic rate, and
294 promoting cell cycle arrest and senescence, and promoted more muted transcriptional expression
295 patterns. TNFR1 signaling was strongly involved in this muted metabolic and inflammatory
296 response since results showed TNFR1 was expressed by all IVD cells and increased with IVDD
297 grade, and since blocking TNFR1 with a CM challenge rescued hAF cell metabolic rate and
298 senescence sufficiently to mount a robust pro-inflammatory response. On the other hand, results
299 supported the hypothesis that TNFR2 signaling was very limited in IVD cells since blocking and
300 Atsttrin had no effects on hAF treated with CM treatment, and since extremely low levels of
301 TNFR2 were measured in IVD cells with qPCR, bulk RNA-seq, scRNA-seq and IHC staining.
302 Meanwhile macrophages expressed TNFR2 at high levels, and αTNFR1 treatment predicted
303 enhanced inflammatory cell recruitment suggesting the immunomodulation of TNFR1 and TNFR2
304 signaling in the IVD may be possible with enhanced interactions of IVD and immune cells.

305 We showed that IVDD tissue from herniation subjects produced high concentrations of
306 several pro-inflammatory cytokines and chemokines that had their largest effects limiting hAF cell
307 metabolic and inflammatory responses. The complex combination of cytokines and chemokines
308 present in IVDD CM are consistent with literature showing a variety of cytokines increase with
309 severity of symptomatic IVD herniation, and that elevated IL-6 plays an important role in painful
310 conditions (11, 51). CM was used to establish and characterize an *in vitro* hAF cell IVDD model
311 capable of promoting and maintaining an IVDD phenotype. The major effects of CM on hAF cells
312 were reduced IVD cell metabolic rates, arrested cell cycle, senescence, and a relatively muted
313 transcriptional response to the complex cytokine and chemokine mixture in CM conditions.
314 Inhibiting TNFR1 enabled hAF cells to sufficiently recover from CM conditions to mount a robust
315 pro-inflammatory response suggesting recovery may be possible under certain conditions. The
316 IVD extracellular matrix is capable of binding cytokines such as TNFα and IL-1β through
317 fibronectin (52), and these cytokines sequestered within the IVD matrix may continue stimulating
318 an IVDD response on affected cells. Individual cytokines can induce premature senescence in IVD
319 cells (17, 53) and this study further shows complex cytokines in CM can arrest hAF cell cycle,
320 induce senescence, and limit IVD cell inflammatory responses independent of nutrient load. The
321 harsh IVDD chemical microenvironment with limited nutrients is often considered a key factor in
322 the 'frustrated' IVD healing response that stimulates the production of chronic pro-inflammatory
323 conditions and results in increased senescence observed with IVDD (54-60). However, IVD cells
324 are adapted to the low oxygen and glucose microenvironment of the IVD and limited nutrients do
325 not explain the reduced hAF cell metabolism from CM challenge in this cell culture study since
326 there were ample nutrients present in CM conditions of all concentrations. We used Basal as
327 control because healthy IVD controls were not available (i.e., surgical samples are degenerated,

328 scoliosis is a different disease process, we do not have access to organ donor samples, and autopsy
329 samples are treated differently and not comparable), and we expect healthy IVD CM would
330 produce effects between the Basal and IVDD CM conditions reported in this study. This study
331 supports the literature showing IVDD cytokines and chemokines play roles inhibiting IVD cell
332 cycle, promoting senescence (17), and inducing a muted transcriptional response in IVDD.

333 IVD cell immunomodulation may be important to arrest IVDD and promote IVD healing,
334 and this study strongly showed a role for TNFR1 since blocking TNFR1 enable hAF cells to mount
335 a robust pro-inflammatory response to the complex CM mixture, even though cell metabolic rate
336 and senescence were only partially rescued. Wang et al., showed a mechanistic role of TNFR1 in
337 IVD healing with significantly improved IVD degeneration score in $TNFR1^{-/-}$ mice (20). The
338 strong TNFR1 immunostaining and increased % positivity with advancing human IVDD grade in
339 this study is similar to prior studies on TNFR1 IHC (31, 61, 62). Translationally, TNFR1-CRISPRi
340 modulation in a rat *in vivo* model improved IVD degeneration and pain response (63). Reduced
341 pain-like behaviors with TNFR1 inhibition are consistent with the depletion of axonogenesis and
342 presynaptic endocytosis identified in this study when blocking the TNFR1 pathway, and suggests
343 TNFR1 may play roles in pain and IVDD. The more robust pro-inflammatory response in this
344 study with TNFR1 inhibition may be beneficial since recent studies suggest acute inflammation is
345 important to promote healing and inhibit chronic pain (64). Further, regenerative healing in
346 tendons requires a more robust and short-term immune response compared to inferior adult healing
347 (65, 66). We believe this study and growing literature suggest that IVD cell immunomodulation
348 with a more acute pro-inflammatory response may be important in shifting IVDD conditions to a
349 more reparative state, and this study builds on the literature suggesting TNFR1 modulation as an
350 important therapeutic target.

351 The limited TNFR2 signaling in IVD cells found in this study was a strong finding
352 supported by qPCR, bulk RNA-seq, scRNA-seq, IHC methods and blocking studies. Lack of
353 TNFR2 signaling in IVD cells has potential for a shift in our understanding of IVD
354 pathophysiology, suggesting IVD cells have limited capacity to mount a repair/regeneration
355 response regardless of their microenvironmental conditions. However, there is a significant body
356 of literature on TNFR2 signaling in the IVD that lacks clarity and needs to be contextualized with
357 this study. For example, TNFR2 IHC was expressed in up to ~ 15% of IVD cells in this study, but
358 the immunostaining was very faint and had no changes in IVD cells with advancing IVDD. Even
359 though review articles suggest TNFR1 and TNFR2 are comparably expressed in the IVD (9, 10),
360 the papers cited are more closely aligned with our findings suggesting limited role for TNFR2.
361 Specifically, TNFR2 was not detectable in AF and NP samples from controls or at very low
362 expression levels and was not increased with IVDD (31, 61, 62). However, TNFR2 levels were
363 increased in human IVDs near defects and in IVDs with immune cells infiltrates (61, 62),
364 suggesting increased TNFR2 signaling in IVDs involves immune cells. The scRNA-seq in this
365 study results support this concept showing *TNFRSF1B* in inflammatory cells but not in IVD cells,
366 and this is supported by our qPCR results showing extremely low *TNFRSF1B* levels in hAF cells.
367 Furthermore, the PanglaoDB scRNA-seq database with over 5M mouse and human cells
368 sequenced shows *TNFRSF1B* is expressed at detectable levels in few cell types, predominantly
369 immune cells including dendritic cells, macrophages and T cells (67). We believe the lack of
370 effects of αTNFR2 and Atsttrin in hAF challenged with CM in this study is best understood if hAF
371 cells indeed have negligible TNFR2 signaling since αTNFR2 had no effects and since Wang et al.,
372 showed that Atsttrin had no effects on $TNFR2^{-/-}$ mice to indicate that Atsttrin is TNFR2-dependent
373 (20). However, TNFR2 signaling is important in IVD degeneration and healing since IVD

374 degeneration increased in TNFR2$^{-/-}$ mice and Atsttrin suppressed TNFα-mediated inflammation in
375 IVD tissue and organ culture models (20, 37). The model systems of these studies showing TNFR2
376 efficacy in IVDD involve immune cells that are capable of robust TNFR2 signaling. Therefore,
377 our results and the literature all point to a very limited role of TNFR2 in IVD cells. However,
378 TNFR2 signaling appears to be important in IVDD progression and most likely involves TNFR2
379 signaling of macrophages and possibly other immune cells.

380 The scRNA-seq analyses identified that the cytokines detected in the multiplex array of
381 IVDD CM were dominantly expressed by a very small population of macrophages and only
382 expressed by native IVD cells at drastically lower levels. Despite substantially lower expression
383 levels in IVD cells, their contribution to the CM cytokines cannot be excluded due to their larger
384 cell numbers in the tissue. The small population of macrophages present were in a predominantly
385 M1 phenotype and also expressed markers (i.e*., ACP5* and *CTSK*, the genes coding for the proteins
386 TRAP and CATHEPSIN K), suggesting their potential osteoclastic origin (Fig. S2D, Fig. S2E)
387 (68). The scRNA-seq results in this study are complementary to human IVDs with IHC identifying
388 small numbers of macrophages infiltrating human IVDDs with a predominantly M1 state that does
389 not convert to a reparative M2 polarization state (55). The small numbers of macrophages isolated
390 in human surgical IVDD in this study further suggests there may be too few immune cells
391 infiltrating the IVDs to enable an effective healing response since inflammatory cell numbers and
392 healing responses depend on species, tissue, timing, and age (69). However, human IVD scRNA-
393 Seq studies are mixed in the number of immune cells identified making this a dynamic area of
394 research and some studies have reported greater numbers of inflammatory cells in human IVDs
395 (70-72). The numbers of immune cells identified in human IVDs will vary depending on
396 degenerative state and isolation methods. We also believe differences in relative abundance of

397 immune cells identified across human IVD scRNA-seq studies are likely related to the annotation
398 methods since IVD cells are known to produce many cytokines and exhibit immune-modulatory
399 behaviors (7, 8, 15, 16, 62), and we had a strict definition of macrophages based on UniCell (45)
400 and lack of IVD cell phenotypic marker expression. An integrated data set and improved precision
401 on phenotypic markers in the immune cell populations present in the IVD in healthy and IVDD
402 conditions are needed to better reconcile differences in relative numbers of macrophages identified
403 across IVD scRNA-seq studies. Regardless, immunomodulation of native IVD cells likely offers
404 more promise for translation since IVD cells are present in much greater numbers than immune
405 cells in the IVD. For example, recently developed bioactive tension-activated nanofiber patches
406 can modulate IVD pro-inflammatory responses through the IL-1β pathway (73), and such
407 approaches can be modified to target additional cytokines and receptors to modulate IVD cell
408 response to the complex IVDD CM environment.

409 In conclusion, results demonstrate distinct roles of TNFR1 and TNFR2 signaling in IVD
410 cell response to IVDD conditions. We show hAF cells subjected to IVDD CM conditions had
411 inhibited metabolic rate, senescence, and a muted inflammatory response. Targeted TNFR1
412 blocking under the CM challenge partially rescued hAF cell MTT response sufficiently to enable
413 them to mount a more robust inflammatory response to CM challenge, with production of many
414 chemokines capable of recruiting immune cells. Meanwhile, native IVD cells appear to lack the
415 capacity for a TNFR2-driven repair under cytokine challenges and must instead rely on recruiting
416 TNFR2 expressing cells, such as macrophages for repair responses. Results point to future
417 therapeutic strategies for painful IVDD involving immunomodulatory strategies for IVD cells
418 including TNFR1 inhibition to restore IVD cell cycle and IVD cell metabolic rates in response to

419 IVDD conditions, and recruitment or delivery of TNFR2 expressing cells that may offer additional
420 benefit for IVD repair.

421 **MATERIALS AND METHODS**

422 **Sex as a biological variable**

423 Our study uses human specimen from both sexes for various experiments (outlined below
424 and in supplementary Tables S1 and S3), but it was not considered a biological variable.

425 **Tissue source**

426 This study was approved by Mount Sinai Institutional Review Board (IRB# STUDY-19-
427 01394-MOD001) project titled 'Orthopedic Cell and Tissue Repository'. For media conditioning,
428 nine human IVDs were obtained from patients (6 males, 3 females), 34-65 years old (mean = 50.4).
429 For cell isolation, six IVDs were obtained (4 males, 2 females), 25-71 years old (mean = 45.8).
430 The collected specimen was assessed, and AF and NP were carefully separated for cell isolation.
431 All patients experienced back or neck pain and underwent disc fusion or discectomy surgery.
432 Assessment of the disease state was performed using Pfirrmann grading on Pre-surgery MRI
433 images. Informed consent from patients was given prior to surgery Specimen information is given
434 in Table S1. Human samples for IHC were obtained from an institutional biobank of cadaveric
435 IVDs. This study included 15 lumbar IVDs (8 Male, 7 Female) (Table S3). The morphological
436 degeneration of each sample was quantified using the Rutgers degeneration scale that ranges from
437 grade 1-12, with 12 as the most degenerated (74). Each sample was graded for Rutgers grade by
438 three trained and independent graders who were blinded to the sample age, sex, and to the Pfirrman
439 grade.

440 **Conditioning of media**

441 Immediately after IVD collection, tissues were cut into smaller pieces, if necessary and
442 washed three times in Phosphate-Buffered Saline (PBS) supplemented with 2% Penicillin /

443 Streptomicin (10,000 U/mL, Gibco) and Primocin (100 µg/mL, Invivogen). Afterwards, the tissue
444 was cultured in 10 mL media (RoosterNourish™-MSC, RoosterBio) per gram tissue and
445 maintained under constant agitation at 37°C and 5% CO_2 for 72 hours. CM was collected and
446 frozen as individual samples at -80°C for later analysis. After initial characterization and analysis
447 of statistical differences between samples, media collected from 9 individuals were combined to
448 reduce number of variables in consecutive experiments.

449 **Media analysis/ Multiplex cytokine array analysis**

450 For quantification of pro-inflammatory cytokines released from surgical samples, media
451 was sampled and analyzed using a Human Cytokine/Chemokine 48-Plex Discovery Assay® Array
452 (catalog no. HD48, Eve Technologies). The 48-Plex Discovery Assay used 100 µL of undiluted
453 cell culture media per run and each run was performed in duplicates. Fluorescence intensity values
454 were derived from the discovery assay and are in direct proportion to the concentration of proteins
455 in the samples.

456 **Isolation and culture of hAF cells**

457 The hAF cells were isolated from surgical specimens. Briefly, collected AF tissue was
458 finely minced and digested using collagenase type I (400 U/mL, Gibco, USA) for 12 hours under
459 constant agitation at 37°C in serum-free high glucose DMEM containing Penicillin / Streptomycin
460 and Amphotericin B (0.25 µg/mL). Using a 70 µm cell strainer debris was removed from the
461 tissue/cell suspension. Cells were either immediately processed for scRNA-seq analysis or seeded
462 at 5,000 cells/cm^2 in RoosterNourish™-MSC media (Rooster Bio) under normoxic (21% O_2)
463 conditions at 37°C and 5 % CO_2 to passage 2-3 to have sufficient cells for CM challenge and
464 blocking experiments. RoosterNourish™-MSC media was selected since it is designed to support
465 high volume expansion of human cells without media changes and therefore had ample nutrients

466 for hAF cell growth under all conditions and obviated the need to adjust nutrient concentrations as
467 we adjusted CM concentration and timing. Specifically, glucose concentration in our media at all
468 CM concentrations ranged 15-40 mM glucose which is several folds greater than the glucose
469 demand for hAF cells in native conditions (46).

470 When primary cells reach 70-80 % confluency, media was changed according to study
471 design (Table 1). Specifically, for Basal group, media was replaced by fresh RoosterNourish™-
472 MSC media (Rooster Bio), for the dosing experiment, CM was diluted using Basal media and for
473 the TNFR blocking experiment, CM was supplemented with anti-TNFR1 (10 µg/mL, MAB225-
474 500, R&D Systems), anti-TNFR2 (10 µg/mL, MAB726-500, R&D Systems) or Atsttrin
475 (200 ng/mL, manufactured in-house). Cultures were moved into a hypoxic environment (5% O_2)
476 for the duration of the experiment and note that cell growth rates did not result in overlapping cells
477 for the 24-72 hour studies performed.

478 **scRNAseq sample preparation and analyses**

479 Immediately after isolation, cells of from 3 patients (5 specimens) were further cleaned up
480 using the LeviCell system (Levitas Bio) according to manufacturer's protocols to remove excess
481 debris. Afterwards, samples were processed according to Chromium 3' Gene Expression V3.1 Kit
482 (10X Genomics, Pleasanton, CA) using manufacturer's guidelines. An estimated 5,000 cells were
483 loaded onto each channel with a targeted cell recovery of approximately 3,000 cells/sample. This
484 was followed by sequencing on a S4 NovaSeq chip (Illumina Inc., San Diego, CA). Qubit 3 (Fisher
485 Scientific) and 2100 Bioanalyzer (Agilent Technologies, Santa Clara, CA) were used for quality
486 check of library.

487 Sequencing data were aligned and quantified using the Cell Ranger Single-Cell Software
488 Suite (version 7.1.0, 10x Genomics) against the reference genome GRCh38. The pipeline grouped

489 and de-duplicated reads confidently mapped to the transcriptome by 10X cellular barcodes and
490 UMIs (Unique Molecular Identifiers), then summarized counts into feature-barcode matrices. The
491 R-based package Seurat (v4.3) was used for further processing and analysis (75). For quality
492 control, standard pre-processing steps were applied to remove cells with <500 mapped genes,
493 <1,000 gene counts, and >20% mitochondrial content. The data were further filtered to removed
494 genes detected in less than 5% of cells per sample. All pre-processed samples were RPCA-
495 integrated using the SCTransform normalization method. The top 4,000 variable features were
496 used to define 20 integration anchors. PCA identified 30 dimensions for unsupervised graph-based
497 clustering via uniform manifold approximation and projection (UMAP) at a 0.5 resolution
498 parameter (76). Genes expressed in >10% of cells in a cluster with an average $\log_2$-fold change
499 >0.25 were selected as DEGs using FindMarkers. Cell types identified from the resulting UMAP
500 were manually annotated based on each cluster's DEG profile and further confirmed using
501 UniCell, an unbiased cell type deconvolution pipeline that leverages a deep learning neural
502 network pre-trained on >28 million annotated single cells from published studies *(43)*. Pathway
503 enrichment was performed using Enrichr to determine significantly enriched biological pathways
504 based on upregulated DEGs, and normalized enrichment scores were reported for top gene
505 pathway sets.

506 **MTT assay**

507 To determine the metabolic activity and respective cell viability, cells were cultured in
508 media, supplemented with 0.5 mg/mL 3-[4,5-dimethylthiazol-2-yl]-2,5-diphenyltetrazolium
509 bromide (MTT, Sigma, USA) for 4 hrs at 37ºC. Afterwards, cells were lysed using Dimethyl
510 Sulfoxide to release insoluble formazan, which was quantified at λ_{ab} = 540 nm with λ_{ref} >650 nm.
511 Absorbance was normalized to basal group to compare between replicates.

512 **Gene expression analysis using qRT-PCR**

513 Quantitative reverse transcription polymerase chain reaction (qRT-PCR) was used to
514 quantify the gene expression of hAF cells that were retained during *in vitro* culture of CM model
515 optimization. RNA was extracted from samples using the RNeasy Micro Kit (QIAGEN INC, USA)
516 according to manufacturer instructions and eluted in 15 µL RNase free water. RNA concentration
517 was quantified using a Thermo Scientific NanoDrop™ One UV–Vis spectrophotometer (Thermo
518 Fisher Scientific) followed by synthesis of complementary DNA (cDNA) using the SuperScript®
519 VILO™ MasterMix (Invitrogen, Waltham, MA) according to manufacturer instructions. The
520 PowerUp™ SYBR™ Green Master Mix (Invitrogen) was used with human primers for
521 Glyceraldehyde 3-Phosphate Dehydrogenase (*GAPDH*, Hs.PT.39a.22214836), Collagen Type I
522 Alpha 1 Chain (*COL1A1*, Hs.PT.58.15517795), ADAM Metallopeptidase with Thrombospondin
523 Type 1 Motif 4 (*ADAMTS4*, Hs.PT.58.19934831), TNF Receptor Superfamily Member 1A
524 (*TNFRSF1A*, Hs.PT.58.19429998) and TNF Receptor Superfamily Member 1B (*TNFRSF1B*,
525 Hs.PT.58.40638488) (all from Integrated DNA Technologies, Coralville IA) according to
526 manufacturer instructions for qRT-PCR. qRT-PCR was performed by the Mount Sinai qPCR
527 CoRE using an ABI PRISM 7900HT sequence detection system with robotic arms (Applied
528 Biosystems, Foster City, CA). Data was analyzed using the $2^{-\Delta\Delta Ct}$ method (77), normalized to
529 housekeeping gene glyceraldehyde 3-phosphate dehydrogenase (GAPDH) and relative to hAF
530 cells cultured basal media. $2^{-\Delta\Delta Ct}$ calculations were conducted using Microsoft Excel (Microsoft,
531 Redmond, NM).

532 **Bulk RNA sequencing and analyses**

533 Bulk RNAseq was used to evaluate changes in gene expression of hAF cells after TNFα
534 signaling modulation ("TNFR blocking"). RNA was extracted from samples using the RNeasy

535 Micro Kit (QIAGEN INC, USA) according to manufacturer instructions with DNase application
536 and eluted in 15 µL RNase free water. RNA concentration was quantified using a Thermo
537 Scientific NanoDrop™ One UV–Vis spectrophotometer (Thermo Fisher Scientific). RNA
538 integrity (RIN) was measured with an Agilent 2100 BioAnalyzer. 2 µg of total RNA from each
539 sample were used for library preparation. Each library was constructed from RNA from hAF cells
540 from 5 individual donors. First, polyadenylated transcripts were enriched using NEXTFLEX
541 Poly(a) Beads 2.0 (PerkinElmer); then, RNA libraries were prepared using the NEXTFLEX®
542 Rapid Directional RNA-Seq Kit 2.0 (PerkinElmer). Library concentration was measure by Qubit,
543 while library quality and size were calculated with an Agilent 2100 BioAnalyzer. Single-end read
544 sequencing was performed using an Illumina NextSeq 550 instrument and a High-output kit, at a
545 depth of 33 million reads per sample.

546 Differential expression of bulk transcriptomic analysis involved several steps. FASTQ files
547 of sequenced reads were aligned to human transcriptome (GENCODE annotation model p10
548 release 27) using the STAR aligner (v2.5.3a), with an average alignment rate of over 80%. Gene-
549 level expression was quantified by the feature Counts (v1.6.3) and normalized by the voom
550 function in R/limma packages. Differential expression was called by R/limma. PCA and clustering
551 were performed in R. Significant DEGs were determined using R/limma at a false discovery rate
552 of 5%, with a fold change greater than or equal to 2. Gene ontology and pathway enrichment was
553 performed using Enrichr to determine significantly enriched or depleted pathways, and normalized
554 enrichment scores reported for top gene ontology and pathway sets.

555 Network analyses used QIAGEN Ingenuity Pathway Analysis (IPA) (QIAGEN Inc.,
556 https://digitalinsights.qiagen.com/IPA) using their developed algorithms (78). Included were
557 DEGs with a FC <-1.5 and >1.5 and a p-value ≤0.01.

558 Heatmaps for cell cycle were created using bulk RNS-seq results and selecting genes
559 recommended for cell cycle analyses with sequencing data that are relevant across multiple cellular
560 models across different biological contexts (49, 50).

561 **Senescence and cell cycle analyses**

562 SA-β-Gal staining was performed using the Senescence Detection Kit (Abcam, ab65351)
563 following the manufacturer's protocol. Briefly, hAF cells were fixed for 15 min with 1× fixation
564 solution, washed with PBS and incubated overnight at 37 °C in 1× staining solution. Brightfield
565 images were captured at 20X on the VWR® Trinocular Inverted Microscope. SA-β-Gal positive
566 cells from 5 biological replicates with n=9 technical replicates per group were analyzed using the
567 ImageJ Cell Counter Plugin.

568 Cleaved-Casp3 staining involved hAF cells fixed in Z-fix formalin fixative for 10 min at
569 room temperature followed by permeabilization for permeabilization using 0.5% TritonX-100 for
570 5 minutes. Cells were incubated for 1 hour at room temperature with serum-free protein block
571 (Dako X0909) to block non-specific binding sites followed by Cleaved-Casp3 primary antibody
572 (Abcam, ab49822, 1:1000) at 4°C over night. Next, the secondary antibody (Cy™5 Donkey Anti-
573 Rabbit IgG, 1:400) (Jackson ImmunoResearch, 711-175-152) was added for 1 hour. Finally,
574 sections were cover slipped using ProLong™ Gold antifade reagent with DAPI (Invitrogen
575 P36931). Dual-channel images were captured at 20X on the Zeiss AxioImager fluorescence
576 microscope. For Co-localization analysis, ImageJ Plugin "EzColocalization" was used to quantify
577 Pearson's correlation coefficient (79). For nuclear fluorescent intensity, the Intensity Density
578 (IntDen) of Casp3 signal within the nuclear reason was determined using ImageJ. A total of 5
579 biological replicates with n=4 technical replicates were analyzed.

580 **IHC analysis of human IVDs**

581 Human specimens were fixed in formaldehyde, embedded in resin, and sectioned in the
582 sagittal plane as previously described (80). Mid-sagittal 5°µm sections from each sample were
583 stained with picrosirius red/alcian blue (PR/AB) for morphological reference. Prior to staining,
584 tissue sections were deplasticized and rehydrated. Sections were then treated with proteinase K
585 (S3020, Dako North America, Carpinteria, CA) followed by protein block (X0909, Dako North
586 America). At room temperature, sections were incubated for one hour with either rabbit polyclonal
587 primary antibody against TNF Receptor 1 (dilution 1:400, ab111119, Abcam, Cambridge, MA),
588 recombinant rabbit monoclonal primary antibody against TNF Receptor 2 [EPR1653] (dilution
589 1:200, ab109322, Abcam, Cambridge, MA) or normal rabbit serum (ab7487, Abcam) as a negative
590 control. Then sections were incubated for 30 minutes at room temperature with anti-rabbit IgG
591 peroxidase secondary antibodies (ImmPRESS reagent, Vector Laboratories, Burlingame, CA).
592 Afterwards the sections were treated with hydrogen peroxide block (ab94710, Abcam) for 10 min
593 followed by diaminobenzidine-based peroxidase substrate for a minute (ImmPACT DAB Vector
594 Laboratories). Finally, the sections were counterstained with 0.1% toluidine blue before mounting.
595 Whole digital slide images were obtained using NanoZoomer S210 from Hamamatsu.
596 Quantification of TNFR1/2 was performed using HALO Image Analysis Platform (v3.6.4134.137,
597 Indica Labs, Albuquerque, NM, USA). Briefly, tissues were annotated to identify the regions to
598 include in the analysis. Once the analysis area is defined, TNFR1/2 is quantified using HALO
599 Multiplex module. The bright filed algorithm uses color deconvolution to separate the
600 chromogenic stains and this allows for the generation of the "markup" image of the of the separated
601 chromogenic stains based on selected settings that will generate the results.

602 **Statistical analyses**

603 The statistical analyses were performed in R (v4.2.3) using R-based package Seurat (v4.3)
604 for analysis of scRNA-seq data and R-based Limma for analysis of bulk RNA-seq data. For all
605 other data, statistical analyses were performed using GraphPad Prism (v10) software. One-way
606 ANOVA or Two-way ANOVA with Tukey's post-tests were used to compare between groups.
607 Results were displayed as mean ± standard deviation. Significance was accepted at a level of $p <$
608 0.05.

609 **ACKNOWLEDGEMENTS**
610 We thank Monica Garcia-barros and the Biorepository and Pathology CoRE at the MSSM
611 for the assistance and contribution of the immunohistochemistry quantification using the HALO
612 software. We thank Dr. Nadine Schrode for her assistance and insights on the scRNA-seq analysis.
613 We thank Dr. Nilsson Holguin for useful discussions on interpretations.

614 **Funding**
615 National Institutes of Health / National Institute of Arthritis and Musculoskeletal and Skin
616 Diseases grant R01AR078857 (JCI). National Institutes of Health / National Institute of Arthritis
617 and Musculoskeletal and Skin Diseases grant R01AR080096 (JCI).

618 **Author contributions**
619 Conceptualization: JCI, JG
620 Study design: JG, EG, JCI
621 Resource acquisition: SC, ACH, WF, CL
622 Performed experiments: JG, EG, DL
623 Analyzed and interpreted the results, and prepared the figures: JG, EG, LR, MW, RS, CL, JCI
624 Funding acquisition: JCI
625 Project administration: JG, JCI
626 Supervision: JCI, JG, RS
627 Writing—original draft: JG, JCI
628 Writing—review, editing and approval: JG, EG, LR, MW, DL, SC, ACH, RS, CL, JCI
629

630 **Competing interests:** Authors declare that they have no competing interests.

631

632 **Data and materials availability:** All data are available in the main text or the supplementary
633 materials. Data and code for RNA-seq analysis will be made available upon manuscript
634 acceptance.
635

636 **REFERENCES**

637 1. Hartvigsen J, Hancock MJ, Kongsted A, Louw Q, Ferreira ML, Genevay S, et al. What
638 low back pain is and why we need to pay attention. *Lancet.* 2018.
639 2. Hoy D, Bain C, Williams G, March L, Brooks P, Blyth F, et al. A systematic review of
640 the global prevalence of low back pain. *Arthritis Rheum.* 2012;64(6):2028-37.
641 3. Hoy D, March L, Brooks P, Blyth F, Woolf A, Bain C, et al. The global burden of low
642 back pain: estimates from the Global Burden of Disease 2010 study. *Ann Rheum Dis.*
643 2014;73(6):968-74.
644 4. Katz JN. Lumbar disc disorders and low-back pain: socioeconomic factors and
645 consequences. *J Bone Joint Surg Am.* 2006;88 Suppl 2:21-4.
646 5. Fujii K, Lai A, Korda N, Hom WW, Evashwick-Rogler TW, Nasser P, et al. *Ex vivo*
647 biomechanics of repaired rat intervertebral discs using genipin crosslinked fibrin adhesive
648 hydrogel. *J Biomech.* 2020;113:110100.
649 6. Iatridis JC, Nicoll SB, Michalek AJ, Walter BA, and Gupta MS. Role of biomechanics on
650 intervertebral disc degeneration and regenerative therapies: What needs repairing in the
651 IVD and what are promising biomaterials for its repair? *The Spine Journal.* 2012:In
652 Press.
653 7. Bermudez-Lekerika P, Crump KB, Tseranidou S, Nuesch A, Kanelis E, Alminnawi A, et
654 al. Immuno-Modulatory Effects of Intervertebral Disc Cells. *Front Cell Dev Biol.*
655 2022;10:924692.
656 8. Risbud MV, and Shapiro IM. Role of cytokines in intervertebral disc degeneration: pain
657 and disc content. *Nat Rev Rheumatol.* 2014;10(1):44-56.
658 9. Wang C, Yu X, Yan Y, Yang W, Zhang S, Xiang Y, et al. Tumor necrosis factor-alpha: a
659 key contributor to intervertebral disc degeneration. *Acta Biochim Biophys Sin (Shanghai).*
660 2017;49(1):1-13.
661 10. Wang X, Wang H, Yang H, Li J, Cai Q, Shapiro IM, et al. Tumor necrosis factor-alpha-
662 and interleukin-1beta-dependent matrix metalloproteinase-3 expression in nucleus
663 pulposus cells requires cooperative signaling via syndecan 4 and mitogen-activated
664 protein kinase-NF-kappaB axis: implications in inflammatory disc disease. *Am J Pathol.*
665 2014;184(9):2560-72.
666 11. Jacobsen HE, Khan AN, Levine ME, Filippi CG, and Chahine NO. Severity of
667 intervertebral disc herniation regulates cytokine and chemokine levels in patients with
668 chronic radicular back pain. *Osteoarthritis Cartilage.* 2020;28(10):1341-50.
669 12. Le Maitre CL, Freemont AJ, and Hoyland JA. The role of interleukin-1 in the
670 pathogenesis of human intervertebral disc degeneration. *Arthritis Res Ther.*
671 2005;7(4):R732-45.

13. Lai A, Moon A, Purmessur D, Skovrlj B, Laudier DM, Winkelstein BA, et al. Annular puncture with tumor necrosis factor-alpha injection enhances painful behavior with disc degeneration *in vivo*. *Spine J.* 2016;16(3):420-31.
14. Walter BA, Purmessur D, Likhitpanichkul M, Weinberg A, Cho SK, Qureshi SA, et al. Inflammatory Kinetics and Efficacy of Anti-inflammatory Treatments on Human Nucleus Pulposus Cells. *Spine (Phila Pa 1976).* 2015;40(13):955-63.
15. Purmessur D, Freemont AJ, and Hoyland JA. Expression and regulation of neurotrophins in the nondegenerate and degenerate human intervertebral disc. *Arthritis Res Ther.* 2008;10(4):R99.
16. Richardson SM, Purmessur D, Baird P, Probyn B, Freemont AJ, and Hoyland JA. Degenerate human nucleus pulposus cells promote neurite outgrowth in neural cells. *PLoS One.* 2012;7(10):e47735.
17. Silwal P, Nguyen-Thai AM, Mohammad HA, Wang Y, Robbins PD, Lee JY, et al. Cellular Senescence in Intervertebral Disc Aging and Degeneration: Molecular Mechanisms and Potential Therapeutic Opportunities. *Biomolecules.* 2023;13(4).
18. Jiang W, Glaeser JD, Kaneda G, Sheyn J, Wechsler JT, Stephan S, et al. Intervertebral disc human nucleus pulposus cells associated with back pain trigger neurite outgrowth in vitro and pain behaviors in rats. *Sci Transl Med.* 2023;15(725):eadg7020.
19. Wang Y, Che M, Xin J, Zheng Z, Li J, and Zhang S. The role of IL-1beta and TNF-alpha in intervertebral disc degeneration. *Biomed Pharmacother.* 2020;131:110660.
20. Wang S, Sun G, Fan P, Huang L, Chen Y, and Chen C. Distinctive roles of tumor necrosis factor receptor type 1 and type 2 in a mouse disc degeneration model. *J Orthop Translat.* 2021;31:62-72.
21. Walter BA, Likhitpanichkul M, Illien-Junger S, Roughley PJ, Hecht AC, and Iatridis JC. TNFalpha transport induced by dynamic loading alters biomechanics of intact intervertebral discs. *PLoS One.* 2015;10(3):e0118358.
22. Autio RA, Karppinen J, Niinimaki J, Ojala R, Veeger N, Korhonen T, et al. The effect of infliximab, a monoclonal antibody against TNF-alpha, on disc herniation resorption: a randomized controlled study. *Spine (Phila Pa 1976).* 2006;31(23):2641-5.
23. Korhonen T, Karppinen J, Paimela L, Malmivaara A, Lindgren KA, Bowman C, et al. The treatment of disc-herniation-induced sciatica with infliximab: one-year follow-up results of FIRST II, a randomized controlled trial. *Spine (Phila Pa 1976).* 2006;31(24):2759-66.
24. Cohen SP, Bogduk N, Dragovich A, Buckenmaier CC, 3rd, Griffith S, Kurihara C, et al. Randomized, double-blind, placebo-controlled, dose-response, and preclinical safety study of transforaminal epidural etanercept for the treatment of sciatica. *Anesthesiology.* 2009;110(5):1116-26.
25. Sainoh T, Orita S, Miyagi M, Inoue G, Kamoda H, Ishikawa T, et al. Single Intradiscal Administration of the Tumor Necrosis Factor-Alpha Inhibitor, Etanercept, for Patients with Discogenic Low Back Pain. *Pain Med.* 2016;17(1):40-5.
26. Genevay S, Viatte S, Finckh A, Zufferey P, Balague F, and Gabay C. Adalimumab in severe and acute sciatica: a multicenter, randomized, double-blind, placebo-controlled trial. *Arthritis Rheum.* 2010;62(8):2339-46.
27. Goupille P, Mulleman D, Paintaud G, Watier H, and Valat JP. Can sciatica induced by disc herniation be treated with tumor necrosis factor alpha blockade? *Arthritis Rheum.* 2007;56(12):3887-95.

718 28. Jing S, Yang C, Zhang X, Wen S, and Li Y. Efficacy and safety of etanercept in the
719 treatment of sciatica: A systematic review and meta-analysis. *J Clin Neurosci.*
720 2017;44:69-74.
721 29. Freeman BJ, Ludbrook GL, Hall S, Cousins M, Mitchell B, Jaros M, et al. Randomized,
722 double-blind, placebo-controlled, trial of transforaminal epidural etanercept for the
723 treatment of symptomatic lumbar disc herniation. *Spine (Phila Pa 1976).*
724 2013;38(23):1986-94.
725 30. Evashwick-Rogler TW, Lai A, Watanabe H, Salandra JM, Winkelstein BA, Cho SK, et
726 al. Inhibiting tumor necrosis factor-alpha at time of induced intervertebral disc injury
727 limits long-term pain and degeneration in a rat model. *JOR Spine.* 2018;1(2).
728 31. Andrade P, Visser-Vandewalle V, Philippens M, Daemen MA, Steinbusch HW, Buurman
729 WA, et al. Tumor necrosis factor-alpha levels correlate with postoperative pain severity
730 in lumbar disc hernia patients: opposite clinical effects between tumor necrosis factor
731 receptor 1 and 2. *Pain.* 2011;152(11):2645-52.
732 32. Kalliolias GD, and Ivashkiv LB. TNF biology, pathogenic mechanisms and emerging
733 therapeutic strategies. *Nat Rev Rheumatol.* 2016;12(1):49-62.
734 33. Huang J, Yu S, Ji C, and Li J. Structural basis of cell apoptosis and necrosis in TNFR
735 signaling. *Apoptosis.* 2015;20(2):210-5.
736 34. Yang S, Wang J, Brand DD, and Zheng SG. Role of TNF-TNF Receptor 2 Signal in
737 Regulatory T Cells and Its Therapeutic Implications. *Front Immunol.* 2018;9:784.
738 35. Sedger LM, and McDermott MF. TNF and TNF-receptors: From mediators of cell death
739 and inflammation to therapeutic giants - past, present and future. *Cytokine Growth Factor*
740 *Rev.* 2014;25(4):453-72.
741 36. Rajput A, and Ware CF. In: Ralph AB, and Philip DS eds. *Encyclopedia of Cell Biology*.
742 Waltham: Academic Press; 2016:354-63.
743 37. Ding H, Wei J, Zhao Y, Liu Y, Liu L, and Cheng L. Progranulin derived engineered
744 protein Atsttrin suppresses TNF-alpha-mediated inflammation in intervertebral disc
745 degenerative disease. *Oncotarget.* 2017;8(65):109692-702.
746 38. Liu CJ, and Bosch X. Progranulin: a growth factor, a novel TNFR ligand and a drug
747 target. *Pharmacol Ther.* 2012;133(1):124-32.
748 39. Tang W, Lu Y, Tian QY, Zhang Y, Guo FJ, Liu GY, et al. The growth factor progranulin
749 binds to TNF receptors and is therapeutic against inflammatory arthritis in mice. *Science.*
750 2011;332(6028):478-84.
751 40. Zhao YP, Tian QY, Liu B, Cuellar J, Richbourgh B, Jia TH, et al. Progranulin knockout
752 accelerates intervertebral disc degeneration in aging mice. *Sci Rep.* 2015;5:9102.
753 41. Wei JL, Fu W, Ding YJ, Hettinghouse A, Lendhey M, Schwarzkopf R, et al. Progranulin
754 derivative Atsttrin protects against early osteoarthritis in mouse and rat models. *Arthritis*
755 *Res Ther.* 2017;19(1):280.
756 42. Purmessur D, Walter BA, Roughley PJ, Laudier DM, Hecht AC, and Iatridis J. A role for
757 TNFalpha in intervertebral disc degeneration: a non-recoverable catabolic shift. *Biochem*
758 *Biophys Res Commun.* 2013;433(1):151-6.
759 43. Maidhof R, Jacobsen T, Papatheodorou A, and Chahine NO. Inflammation induces
760 irreversible biophysical changes in isolated nucleus pulposus cells. *PLoS One.*
761 2014;9(6):e99621.
762 44. Johnson ZI, Doolittle AC, Snuggs JW, Shapiro IM, Le Maitre CL, and Risbud MV. TNF-
763 alpha promotes nuclear enrichment of the transcription factor TonEBP/NFAT5 to

764 selectively control inflammatory but not osmoregulatory responses in nucleus pulposus
765 cells. *J Biol Chem.* 2017;292(42):17561-75.
766 45. Charytonowicz D, Brody R, and Sebra R. Interpretable and context-free deconvolution of
767 multi-scale whole transcriptomic data with UniCell deconvolve. *Nat Commun.*
768 2023;14(1):1350.
769 46. McDonnell EE, and Buckley CT. Two- and three-dimensional in vitro nucleus pulposus
770 cultures: An in silico analysis of local nutrient microenvironments. *JOR Spine.*
771 2022;5(3):e1222.
772 47. Tye BK. MCM proteins in DNA replication. *Annu Rev Biochem.* 1999;68:649-86.
773 48. Han L, Chen Z, Yu K, Yan J, Li T, Ba X, et al. Interleukin 27 Signaling in Rheumatoid
774 Arthritis Patients: Good or Evil? *Front Immunol.* 2021;12:787252.
775 49. Whitfield ML, Sherlock G, Saldanha AJ, Murray JI, Ball CA, Alexander KE, et al.
776 Identification of genes periodically expressed in the human cell cycle and their
777 expression in tumors. *Mol Biol Cell.* 2002;13(6):1977-2000.
778 50. Riba A, Oravecz A, Durik M, Jimenez S, Alunni V, Cerciat M, et al. Cell cycle gene
779 regulation dynamics revealed by RNA velocity and deep-learning. *Nat Commun.*
780 2022;13(1):2865.
781 51. Weber KT, Alipui DO, Sison CP, Bloom O, Quraishi S, Overby MC, et al. Serum levels
782 of the proinflammatory cytokine interleukin-6 vary based on diagnoses in individuals
783 with lumbar intervertebral disc diseases. *Arthritis Res Ther.* 2016;18:3.
784 52. Vaday GG, Hershkoviz R, Rahat MA, Lahat N, Cahalon L, and Lider O. Fibronectin-
785 bound TNF-alpha stimulates monocyte matrix metalloproteinase-9 expression and
786 regulates chemotaxis. *J Leukoc Biol.* 2000;68(5):737-47.
787 53. Feng C, Liu H, Yang M, Zhang Y, Huang B, and Zhou Y. Disc cell senescence in
788 intervertebral disc degeneration: Causes and molecular pathways. *Cell Cycle.*
789 2016;15(13):1674-84.
790 54. Adams MA, Lama P, Zehra U, and Dolan P. Why do some intervertebral discs
791 degenerate, when others (in the same spine) do not? *Clin Anat.* 2015;28(2):195-204.
792 55. Nakazawa KR, Walter BA, Laudier DM, Krishnamoorthy D, Mosley GE, Spiller KL, et
793 al. Accumulation and localization of macrophage phenotypes with human intervertebral
794 disc degeneration. *Spine J.* 2018;18(2):343-56.
795 56. Huang YC, Urban JP, and Luk KD. Intervertebral disc regeneration: do nutrients lead the
796 way? *Nat Rev Rheumatol.* 2014;10(9):561-6.
797 57. Le Maitre CL, Freemont AJ, and Hoyland JA. Accelerated cellular senescence in
798 degenerate intervertebral discs: a possible role in the pathogenesis of intervertebral disc
799 degeneration. *Arthritis Res Ther.* 2007;9(3):R45.
800 58. Yee A, Lam MP, Tam V, Chan WC, Chu IK, Cheah KS, et al. Fibrotic-like changes in
801 degenerate human intervertebral discs revealed by quantitative proteomic analysis.
802 *Osteoarthritis Cartilage.* 2016;24(3):503-13.
803 59. Patil P, Niedernhofer LJ, Robbins PD, Lee J, Sowa G, and Vo N. Cellular senescence in
804 intervertebral disc aging and degeneration. *Curr Mol Biol Rep.* 2018;4(4):180-90.
805 60. Yurube T, Takeoka Y, Kanda Y, Kuroda R, and Kakutani K. Intervertebral disc cell fate
806 during aging and degeneration: apoptosis, senescence, and autophagy. *N Am Spine Soc J.*
807 2023;14:100210.
808 61. Bachmeier BE, Nerlich AG, Weiler C, Paesold G, Jochum M, and Boos N. Analysis of
809 tissue distribution of TNF-alpha, TNF-alpha-receptors, and the activating TNF-alpha-

converting enzyme suggests activation of the TNF-alpha system in the aging intervertebral disc. *Ann N Y Acad Sci.* 2007;1096:44-54.
62. Phillips KL, Chiverton N, Michael AL, Cole AA, Breakwell LM, Haddock G, et al. The cytokine and chemokine expression profile of nucleus pulposus cells: implications for degeneration and regeneration of the intervertebral disc. *Arthritis Res Ther.* 2013;15(6):R213.
63. Stover JD, Trone MAR, Weston J, Lewis C, Levis H, Philippi M, et al. Therapeutic TNF-alpha Delivery After CRISPR Receptor Modulation in the Intervertebral Disc. *bioRxiv.* 2023:2023.05.31.542947.
64. Parisien M, Lima LV, Dagostino C, El-Hachem N, Drury GL, Grant AV, et al. Acute inflammatory response via neutrophil activation protects against the development of chronic pain. *Sci Transl Med.* 2022;14(644):eabj9954.
65. Chazaud B. Inflammation and Skeletal Muscle Regeneration: Leave It to the Macrophages! *Trends Immunol.* 2020;41(6):481-92.
66. Howell KL, Kaji DA, Li TM, Montero A, Yeoh K, Nasser P, et al. Macrophage depletion impairs neonatal tendon regeneration. *FASEB J.* 2021;35(6):e21618.
67. Franzen O, Gan LM, and Bjorkegren JLM. PanglaoDB: a web server for exploration of mouse and human single-cell RNA sequencing data. *Database (Oxford).* 2019;2019.
68. Takeshita S, Kaji K, and Kudo A. Identification and characterization of the new osteoclast progenitor with macrophage phenotypes being able to differentiate into mature osteoclasts. *J Bone Miner Res.* 2000;15(8):1477-88.
69. Eming SA, Wynn TA, and Martin P. Inflammation and metabolism in tissue repair and regeneration. *Science.* 2017;356(6342):1026-30.
70. Chen F, Lei L, Chen S, Zhao Z, Huang Y, Jiang G, et al. Serglycin secreted by late-stage nucleus pulposus cells is a biomarker of intervertebral disc degeneration. *Nat Commun.* 2024;15(1):47.
71. Cherif H, Mannarino M, Pacis AS, Ragoussis J, Rabau O, Ouellet JA, et al. Single-Cell RNA-Seq Analysis of Cells from Degenerating and Non-Degenerating Intervertebral Discs from the Same Individual Reveals New Biomarkers for Intervertebral Disc Degeneration. *Int J Mol Sci.* 2022;23(7).
72. Gan Y, He J, Zhu J, Xu Z, Wang Z, Yan J, et al. Spatially defined single-cell transcriptional profiling characterizes diverse chondrocyte subtypes and nucleus pulposus progenitors in human intervertebral discs. *Bone Res.* 2021;9(1):37.
73. Peredo AP, Gullbrand SE, Friday CS, Orozco BS, Dehghani B, Jenk AC, et al. Tension-activated nanofiber patches delivering an anti-inflammatory drug improve repair in a goat intervertebral disc herniation model. *Sci Transl Med.* 2023;15(722):eadf1690.
74. Rutges JP, Duit RA, Kummer JA, Bekkers JE, Oner FC, Castelein RM, et al. A validated new histological classification for intervertebral disc degeneration. *Osteoarthritis Cartilage.* 2013;21(12):2039-47.
75. Satija R, Farrell JA, Gennert D, Schier AF, and Regev A. Spatial reconstruction of single-cell gene expression data. *Nat Biotechnol.* 2015;33(5):495-502.
76. Shaath H, Vishnubalaji R, Elkord E, and Alajez NM. Single-Cell Transcriptome Analysis Highlights a Role for Neutrophils and Inflammatory Macrophages in the Pathogenesis of Severe COVID-19. *Cells.* 2020;9(11).
77. Livak KJ, and Schmittgen TD. Analysis of relative gene expression data using real-time quantitative PCR and the 2(-Delta Delta C(T)) Method. *Methods.* 2001;25(4):402-8.

856 78. Kramer A, Green J, Pollard J, Jr., and Tugendreich S. Causal analysis approaches in
857 Ingenuity Pathway Analysis. *Bioinformatics.* 2014;30(4):523-30.
858 79. Stauffer W, Sheng H, and Lim HN. EzColocalization: An ImageJ plugin for visualizing
859 and measuring colocalization in cells and organisms. *Sci Rep.* 2018;8(1):15764.
860 80. Walter BA, Torre OM, Laudier D, Naidich TP, Hecht AC, and Iatridis JC. Form and
861 function of the intervertebral disc in health and disease: a morphological and stain
862 comparison study. *J Anat.* 2015;227(6):707-16.
863
864

FIGURES & LEGENDS

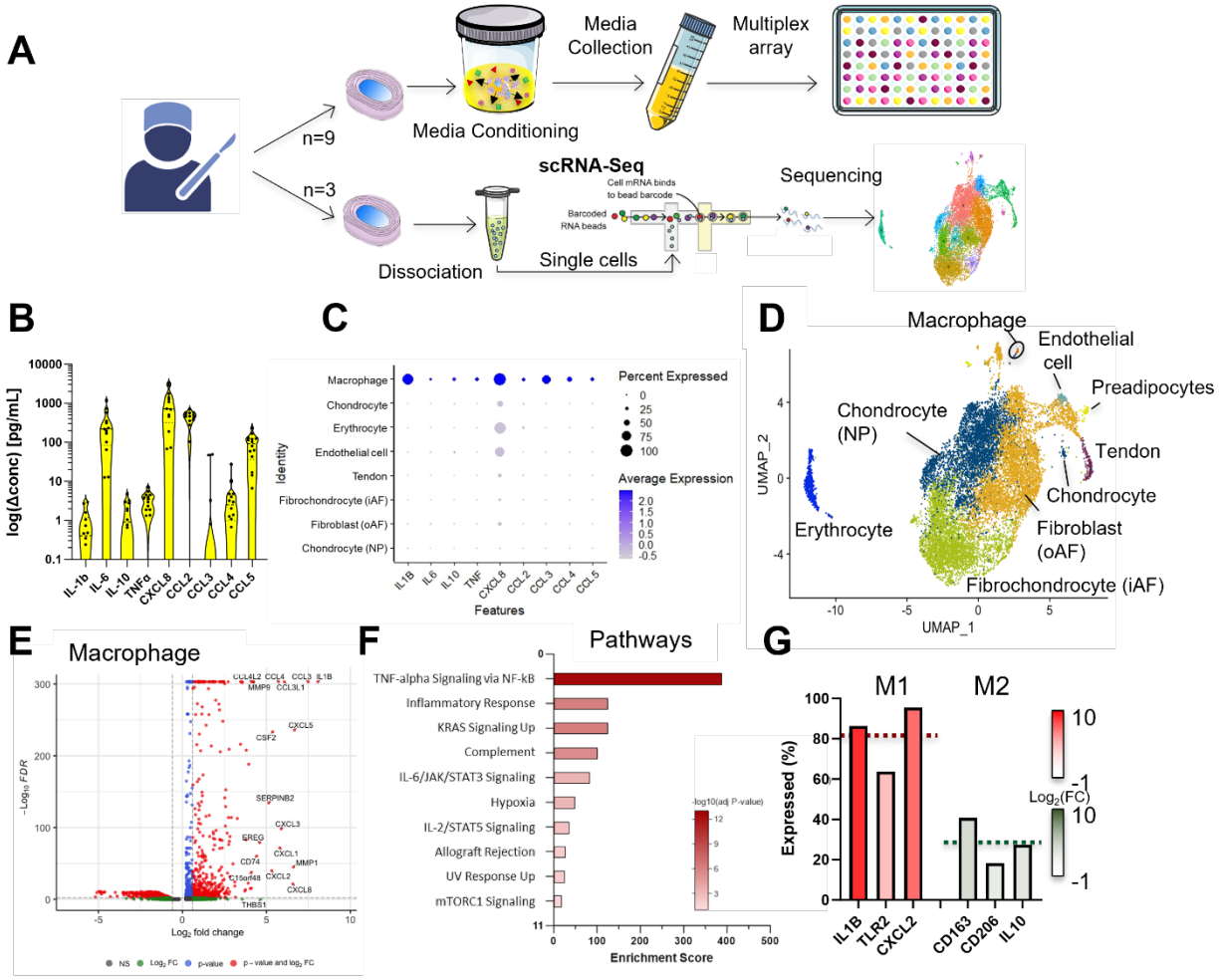

FIGURE 1

Fig. 1. Painful human IVDD tissue contains high concentrations chemokines and cytokines, dominantly expressed from a small population of M1 macrophages highly enriched for TNF-alpha signaling. (A) Specimen from subjects were collected and either used for CM generation and characterization (top) or for cell dissociation and scRNA-seq analysis (bottom). (B) IVDD CM contains a complex array of pro- and anti-inflammatory cytokines and chemokines. (C) IVDD cytokines are dominantly expressed by macrophage sub-population of IVD cells with surprisingly little expression in other IVDD cell populations. (D) UMAP of IVDD cells annotated with UniCell Deconvolve identified 7 cell types including a small population of macrophages. Since relatively few IVD studies are included in the UniCell Deconvolve training set, we parenthetically added IVD-specific annotations to the UMAP. (E) Volcano plot shows DEGs with pro-inflammatory genes CCL3, CCL4 and IL1B as most significantly upregulated genes, which contribute to (F) pathways analysis revealing TNF-alpha signaling as the most significant and highest enriched pathway of this population. (G) M1/M2 macrophage polarization quantification showed a 3-fold higher amount of M1 macrophages within the IVD.

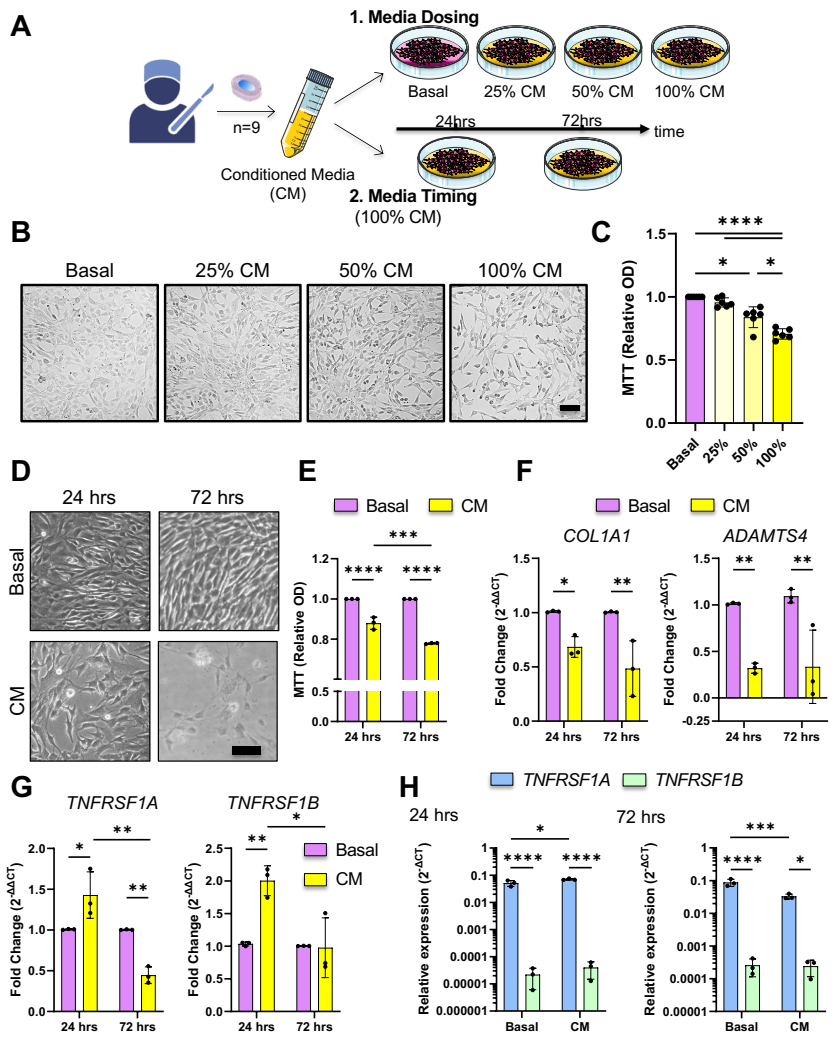

FIGURE 2

Fig. 2. Human AF cell IVDD model system shows CM reduces MTT metabolic activity and modulates TNFR1 and TNFR2 responses. (A) CM generated from 9 subjects were first applied in different dosages (0-100%) for 24 hours ("Media Dosing"), followed by culture for 24 hours and 72 hours respectively ("Media Timing") (B) Cell growth area decreases with increasing concentration of CM, which is reflected in (C) where cell proliferation significantly decreases with increasing CM, indicated by MTT assay. (D) Culturing hAF cells for 72 hours in CM has a detrimental effect on cell growth and morphology compared to Basal and 24 hours CM exposure, which is also seen in (E) with significantly lower relative OD, indicating lower cell growth, and (F) reduced *COL1A1* and *ADAMTS4* expression, and limited inflammatory response (Fig. S3). (G) hAF cell culture in CM for 24 hours significantly increases gene expression *TNFRSF1A* (gene for TNFR1) and *TNFRSF1B* (gene for TNFR2) compared to Basal and 72 hours culture. (H) Relative gene expression normalized to *GAPDH* of *TNFRSF1A* and *TNFRSP1B* after 24 and 72 hours ($2^{-\Delta CT}$). *, **, *** and **** represent significant differences between groups with $p < 0.05$, 0.01, 0.001 and 0.0001 respectively. Scale bar = 100 µm.

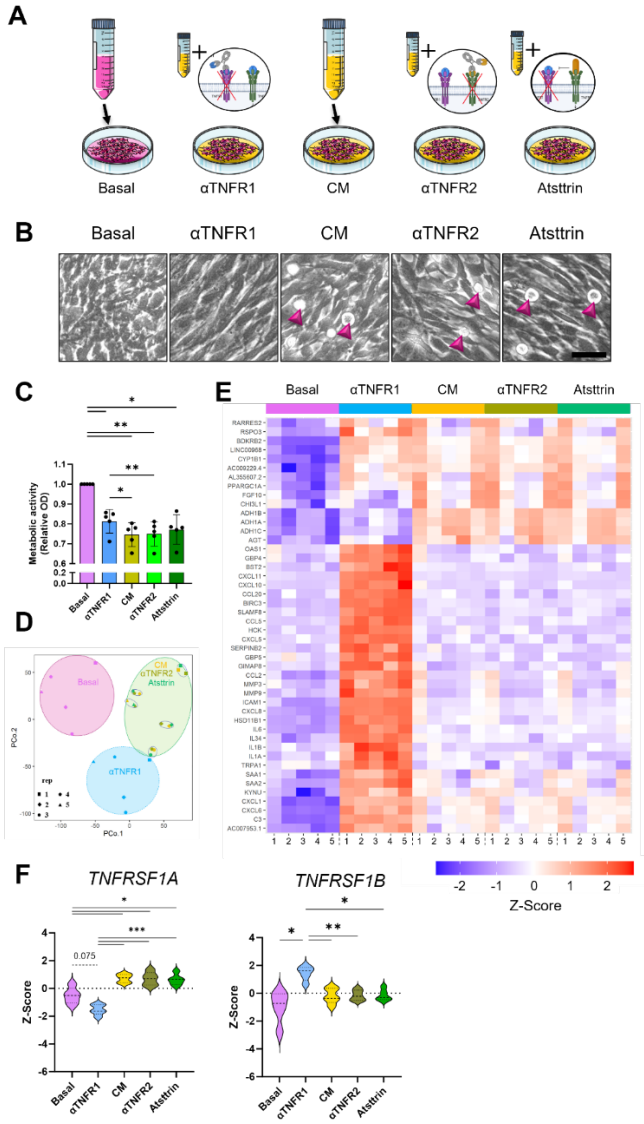

FIGURE 3

Fig. 3. TNFR1 blocking of hAF cells with IVDD CM partially rescues metabolic rate and expresses a pro-inflammatory transcriptome while TNFR2 blocking and Atsttrin had no effects. (A) Cells were either cultured for 24 hours in Basal media, CM or CM supplemented with αTNFR1, TNFR2 or Atsttrin respectively. (B) hAF cells in CM, αTNFR2 and Atsttrin show greater number of floating dead cells (arrowheads), which is consistent with (C) reduced cell growth/viability in CM, αTNFR2 and Atsttrin compared to basal, which was partly recovered in αTNFR1. (D) Distinct transcriptomic difference between Basal, αTNFR1 and all other groups are apparent in PCA plot, and (E) heatmap, which shows a clear change in top DRG patterns with many pro-inflammatory genes among the top 50 DEGs. (F) Gene expression of TNFR1 is significantly downregulated upon TNFR1 blocking, whereas TNFR2 is upregulated. *, ** and *** represent significant differences between groups with $p < 0.05$, 0.01 and 0.001 respectively. Scale bar = 50 µm.

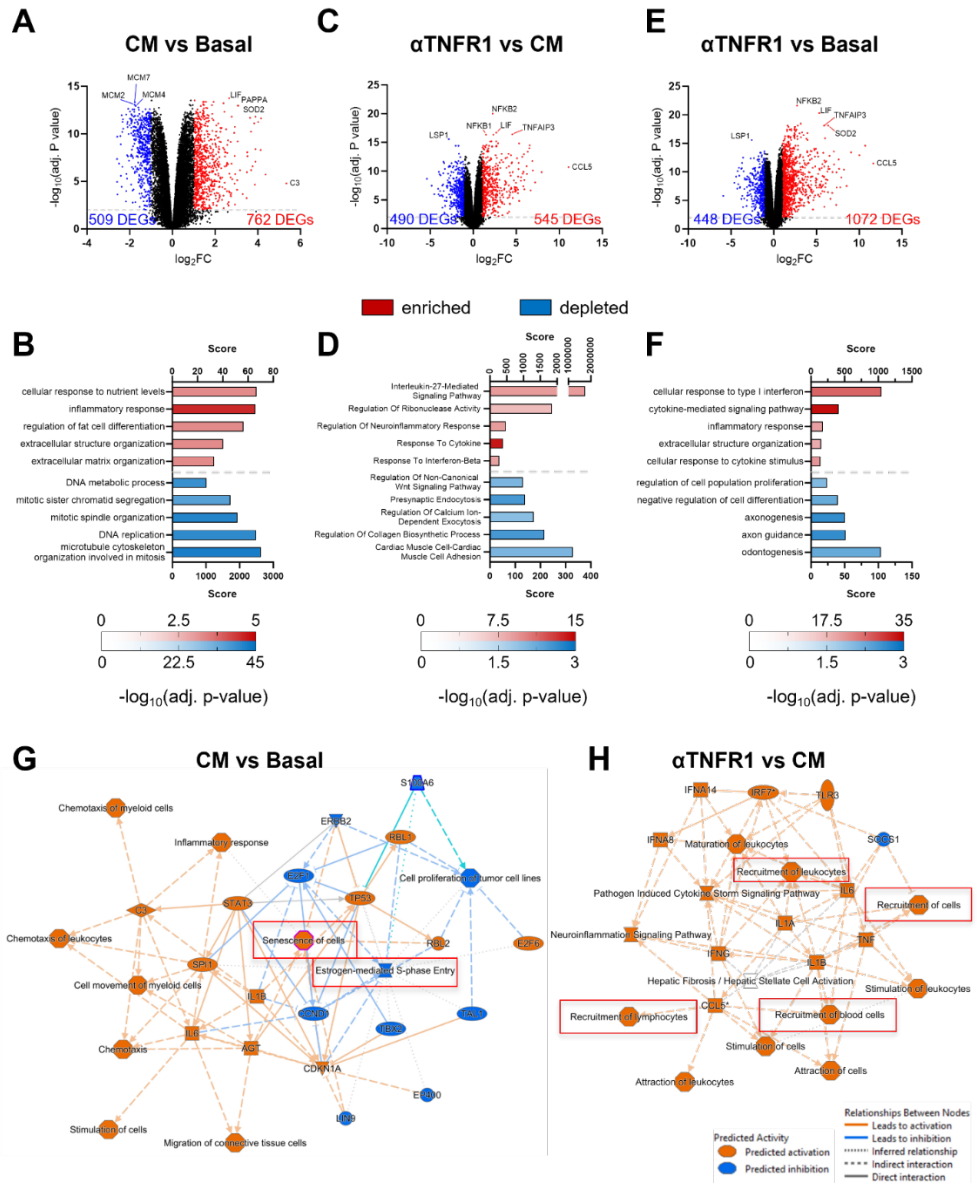

FIGURE 4

Fig. 4. CM reduces mitotic responses while TNFR1 inhibition promotes processes for immune cell recruitment. (A) 509 of 1271 DEGs in CM were significantly downregulated compared to Basal. (B) Biological processes depleted upon CM were related to DNA replication and mitosis. (C) Comparing αTNFR1 to CM, 454/1035 DEGs were significantly upregulated. (D) Biological processes modulated by αTNFR1were related to an enrichment of IL-27 signaling and RNase activity. (E) Volcano plot comparing αTNFR1 to Basal significantly upregulated 1072/1520 DEGs. (D) Hereby, biological processes related to cytokine signaling and inflammatory responses were enriched, while axonogenesis and axon guidance was depleted. (G) Qiagen IPA analysis of CM vs Basal predicted an activation of senescence while proliferation was inhibited. (H) Inhibition of TNFR1 activates processes related to immune-cell recruitment in IPA analysis.

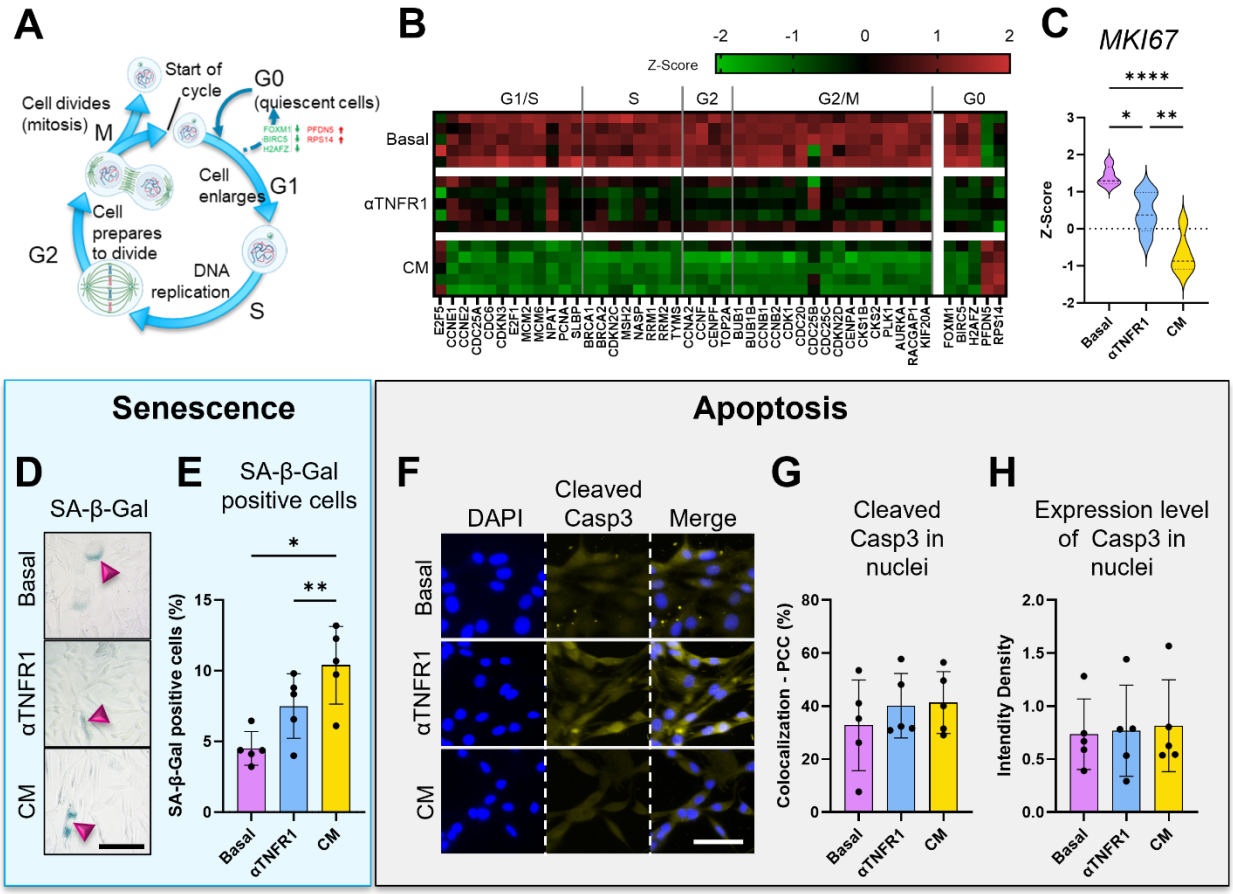

FIGURE 5

Fig. 5. IVDD CM inhibited active hAF cell mitosis and promoted senescence that was partially prevented with TNFR1 inhibition. (A) Schematic of different stages of the cell cycle. (B) Heatmaps using transcripts selected to study cell cycle in multiple cellular models and different biological contexts (49, 50) showed Basal activated hAF cell cycle while CM caused expression of G0 phase transcripts. (C) MKI67 proliferation marker was significantly decreased in CM compared to Basal and αTNFR1. (D) SA-β-Gal staining of hAF cells was (E) significantly higher in CM compared to Basal and αTNFR1. (F) Staining for cleaved Casp3 showed (G) no difference in co-localization of cleaved Casp3 and DAPI and (H) no difference nuclear cleaved Casp3 intensity density. *, ** and **** represented $p < 0.05$, 0.01 and 0.0001, respectively. Scale bar = 50 µm.

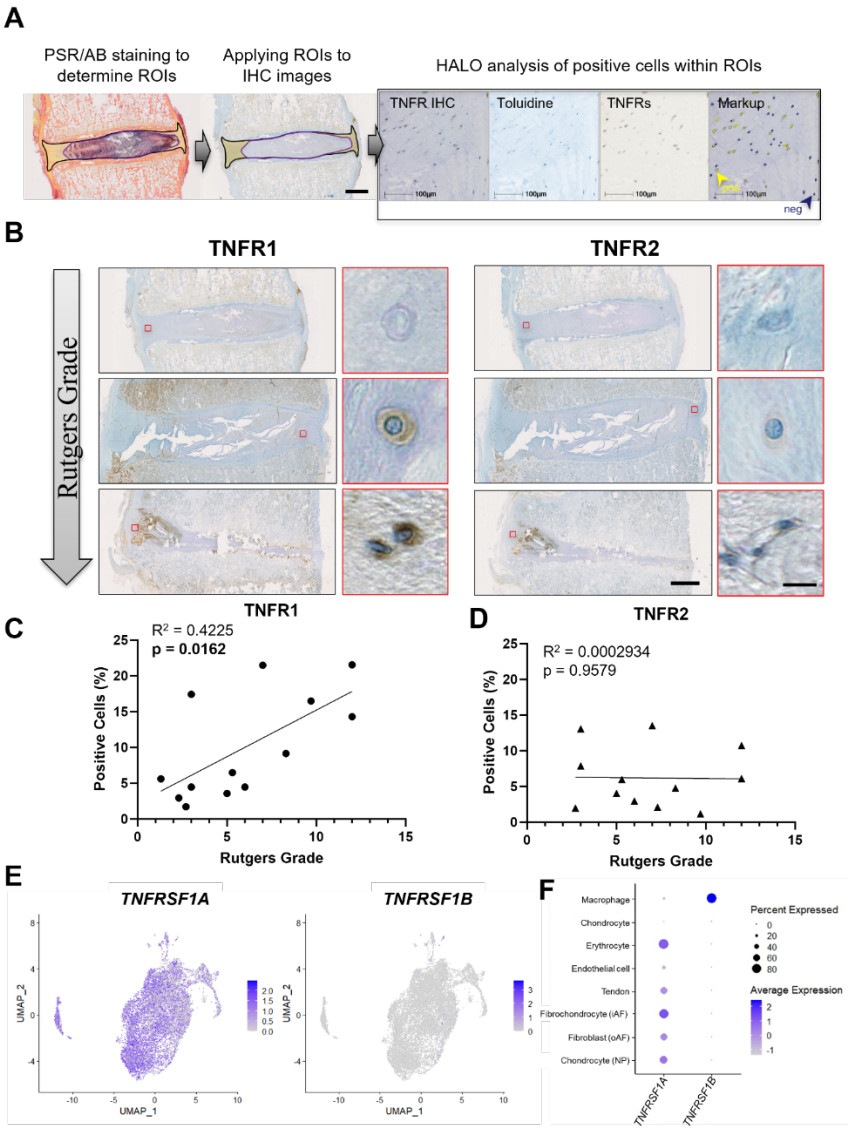

FIGURE 6

Fig. 6. TNFR1 expression was expressed in all IVD cells and correlated with IVD degeneration grade while TNFR2 was only expressed in macrophages and not IVD cells. (A) Analysis of IHC was performed using HALO Multiplex module, whereby the oAF region was determined using PSR/AB staining and the ROI overlayed onto TNFR1/2 IHC imaged for follow up AI-based analysis. (B) Intensity and quantity of TNFR1 increases with Rutgers degeneration grade, while TNFR2 shows faint staining across degeneration. (C) Correlation between TNFR1 positive cells and Rutgers grade is significant (p=0.0162), while (D) there is no correlation with TNFR2 positive cells and Rutgers grade. (E) UMAP of herniated IVD specimen showed TNFR1 expression across cell populations and little TNFR2 expression. (F) TNFR2 is expressed exclusively in macrophage-derived cell population. Scale bar (full IVD) = 5 mm, Scale bar (AF cell) = 10 µm.

963 **Table 1. Experimental groups for *in vitro* hAF cell culture experiments**

	Groups and supplements		Duration
Dosing	Basal	-	24 hours
	CM	25% 50% 100%	
Timing	Basal	-	24 hours 72 hours
	CM	100%	
TNFR blocking	Basal	-	24 hours
	CM	-	
	CM + αTNFR1	10 µg/mL	
	CM + αTNFR2	10 µg/mL	
	CM + Atsttrin	200 ng/mL	

964